Vertically coupled microring resonators using one epitaxial growth step and single-side lithography

Óscar García López,[1,3,*] Dries Van Thourhout,[2] Daniel Lasaosa,[1] Manuel López-Amo,[1] Roel Baets,[2] and Marko Galarza[1]

[1]*Department of Electric and Electronic Engineering, Universidad Pública de Navarra,Campus Arrosadia s/n, 31006 Pamplona, Spain*

[2]*Department of Information Technology, Photonics Research Group, Ghent University, 9000 Gent, Belgium*

[3]*Fundación Cetena, 31110 Noain, Spain*

[*]*ogarcialo@gmail.com*

Abstract: A new concept for the fabrication of integrated microring resonators, requiring only one single epitaxial growth and two single-side lithographic steps, is proposed in what is the simplest fabrication scheme for vertical microrings published to date. The approach is based on two vertically stacked phase matched core layers. The effect of bus waveguide, coupling region and ring structure parameters is theoretically analyzed. Numerical calculations predict high performance devices with quality factors of over 10000. The scheme can feature both active and passive regions, allowing the fabrication of microring lasers.

OCIS codes: (130.0130) Integrated optics; (130.3120) Integrated optics devices.

References and links

1. M. C. M. M. Souza, L. A. M. Barea, F. Vallini, G. F. M. Rezende, G. S. Wiederhecker, and N. C. Frateschi, "Embedded coupled microrings with high-finesse and close-spaced resonances for optical signal processing," Opt. Express **22**(9), 10430–10438 (2014).
2. X. M. Lv, Y. D. Yang, L. X. Zou, H. Long, J. L. Xiao, Y. Du, and Y. Z. Huang, "Mode characteristics and optical bistability for AlGaInAs/InP microring lasers," IEEE Photon. Technol. Lett. **26**(17), 1703–1706 (2014).
3. W. D. Sacher, W. M. J. Green, D. M. Gill, S. Assefa, T. Barwicz, M. Khater, E. Kiewra, C. Reinholm, S. M. Shank, Y. A. Vlasov, and J. K. S. Poon, "Binary phase-shift keying by coupling modulation of microrings," Opt. Express **22**(17), 20252–20259 (2014).
4. R. D. Mansoor, H. Sasse, M. Al Asadi, S. J. Ison, and A. P. Duffy, "Over coupled ring resonator-based add/drop filters," IEEE J. Quantum Electron. **50**(8), 598–604 (2014).
5. B. Yang, A. Shen, C. Qiu, T. Hu, L. Yang, H. Yu, X. Jiang, Y. Li, Y. Hao, and J. Yang, "Microring-based ratio-metric wavelength monitor on silicon," Opt. Lett. **39**(11), 3298–3300 (2014).
6. A. Fushimi and T. Tanabe, "All-optical logic gate operating with single wavelength," Opt. Express **22**(4), 4466–4479 (2014).
7. P. P. Absil, J. V. Hryniewicz, B. E. Little, F. G. Johnson, K. J. Ritter, and P. T. Ho, "Vertically coupled microring resonators using polymer wafer bonding," IEEE Photon. Technol. Lett. **13**(1), 49–51 (2001).
8. A. Kapsalis, I. Stamataki, C. Mesaritakis, D. Syvridis, M. Hamacher, and H. Heidrich, "Design and experimental evaluation of active-passive integrated microring lasers: threshold current and spectral properties," IEEE J. Quantum Electron. **47**(12), 1557–1564 (2011).
9. S. J. Choi, K. Djordjev, S. J. Choi, P. D. Dapkus, W. Lin, G. Griffel, R. Menna, and J. Connolly, "Microring resonators vertically coupled to buried heterostructure bus waveguides," IEEE Photon. Technol. Lett. **16**(3), 828–830 (2004).
10. C. W. Tee, K. A. Williams, R. V. Penty, I. H. White, and M. Hamacher, "Noncritical waveguide alignment for vertically coupled microring using a mode-expanded bus architecture," IEEE Photon. Technol. Lett. **18**(20), 2129–2131 (2006).
11. O. G. López, D. Lasaosa, M. López-Amo, and M. Galarza, "Highly-efficient fully resonant vertical couplers for InP active-passive monolithic integration using vertically phase matched waveguides," Opt. Express **21**(19), 22717–22727 (2013).
12. M. Heinbach, M. Schienle, A. Schmid, B. Acklin, and G. Müller, "Low-loss bent connections for optical switches," J. Lightwave Technol. **15**(5), 833–837 (1997).

#230578 - $15.00 USD Received 17 Dec 2014; revised 4 Feb 2015; accepted 5 Feb 2015; published 20 Feb 2015

13. W. Huang, "Coupled-mode theory for optical waveguides: an overview," J. Opt. Soc. Am. A **11**(3), 963–983 (1994).
14. Fimmwave (Photon Design), [http://www.photond.com].
15. C. W. Tee, K. A. Williams, R. V. Penty, and I. H. White, "Fabrication-tolerant active-passive integration scheme for vertically coupled microring resonator," IEEE J. Sel. Top. Quantum Electron. **12**(1), 108–116 (2006).
16. S. J. Choi, K. Djordjev, Z. Peng, Q. Yang, S. J. Choi, and P. D. Dapkus, "Laterally coupled buried heterostructure high-Q ring resonators," IEEE Photon. Technol. Lett. **16**(10), 2266–2268 (2004).
17. C. Vassallo and J. M. van der Keur, "Comparison of a few transparent boundary conditions for finite-difference optical mode-solvers," J. Lightwave Technol. **15**(2), 397–402 (1997).

1. Introduction

Microring resonators are key building blocks in the structure of a large variety of photonic integrated devices. Thanks to their sharp wavelength selectivity and compact feature size, microring resonators are suitable for numerous optical applications such as filtering [1], lasing [2], modulation [3], routing [4], optical processing [5] and all optical logic gates [6]. The basic layout of a ring resonator consists of a circular waveguide and two tangential straight waveguides serving as evanescent wave input and output couplers to the ring. The ring radius is defined by the functionality of the device, whereas the coupler geometry offers two structural possibilities: laterally coupled and vertically coupled microring resonators.

In the lateral approach, the microring and the bus waveguides lie on the same horizontal plane, implying certain drawbacks. First, the coupling gap between the microring and the bus waveguides usually needs to be submicron, requiring electron beam lithography in order to ensure sufficient coupling. Such small features results in nanometric tolerances in the microring design, making it difficult to achieve reproducible device performance. Next, the fact that the microring and bus waveguides are defined in the same epitaxial growth drastically limits the flexibility in the device design. In this case, achieving functionalities which require active-passive integration results in a dramatic complexity increase in the fabrication process.

In order to overcome these issues, vertically coupled ring resonators have been investigated exhaustively over recent years [7]. With vertically coupled ring resonators, the layer structure contains two vertically stacked waveguide core layers, one to define the bus waveguides and the other for the microring. Vertical spatial distribution allows for the definition of active-passive structures, using one single epitaxial growth to define the passive bus waveguides and the active microring. Furthermore, since the coupling between the bus and the ring waveguides mainly depends on the thickness of the intermediate layer, which is accurately determined by the epitaxial growth, it can be controlled more precisely than it can in laterally coupled microring resonators.

The first disadvantage of vertically coupled microring resonators is the increased complexity of fabrication because wafer bonding [8] or regrowth [9] is usually required in order to manufacture such devices. A second disadvantage is the fact that two lithography steps are required either on each side of the wafer or after each growth step, making alignment a critical issue [10].

In this paper a new concept for regrowth- and wafer-bonding-free vertically coupled microring resonators is presented. The proposed structure is based on two vertically coupled phase matched waveguides. One single epitaxial growth and two single-side standard photolithographic steps are required in what is the simplest fabrication scheme for vertical microrings published to date. The approach is suitable for either only-passive or active-passive functionalities and is compatible with the integration scheme proposed by the authors in [11].

2. Concept

A three dimensional representation of the proposed device is shown in Fig. 1. The vertical confinement of light is achieved by means of two vertically stacked phase matched cores. The lower core is used to define the bus waveguide, whereas the upper core provides the optical

#230578 - $15.00 USD Received 17 Dec 2014; revised 4 Feb 2015; accepted 5 Feb 2015; published 20 Feb 2015

guiding in the ring. In section A, only the lower bus waveguide is defined. It is smoothly bent and tapered in order to efficiently transform the guided bus mode into the main whispering gallery mode of the disk bus structure in section B. In section B there is no need for the inner sidewall of the waveguide for an ultra-low loss propagation of light. This geometrical feature allows the definition of the ring over the bent bus waveguide. Section C provides the evanescent coupling between the bus whispering gallery mode and the upper ring mode. Light coupled to the ring is totally confined in the upper core because the underlying quasi-slab waveguide provided by the unetched bus core drastically breaks the phase matching condition between both waveguides [11]. The optical modes taking part in each section are shown in the insets of Fig. 1.

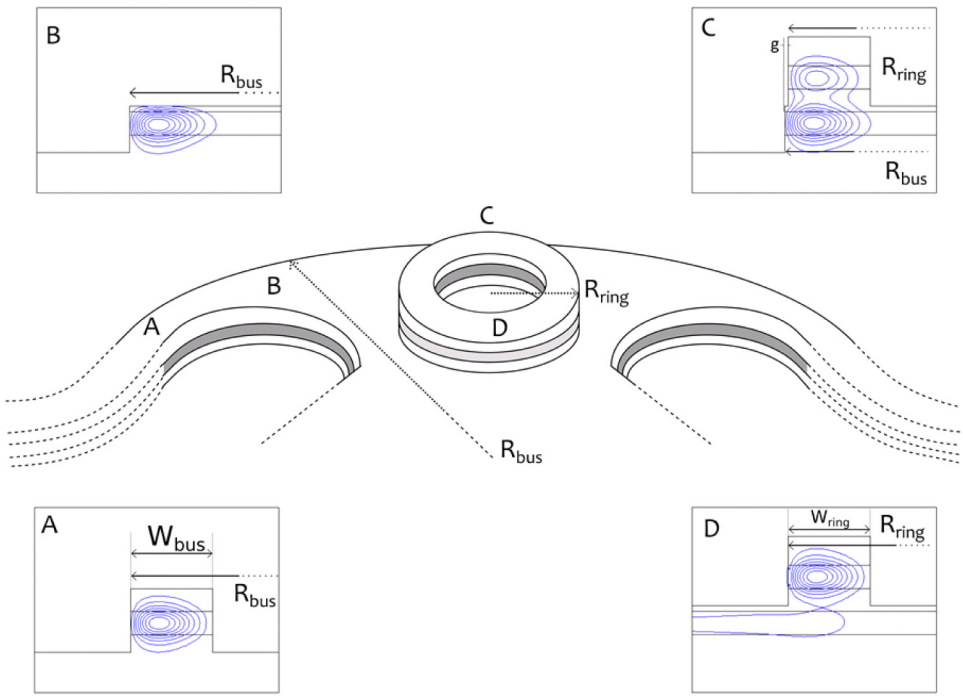

Fig. 1. Schematic drawing of the proposed microring. The insets show the field distribution of the propagation modes in the bus waveguide (A), the disk bus waveguide (B), the coupling region (C1, C2) and the ring waveguide (D).

3. Design and simulation results

3.1 Waveguide design

The epitaxial layer structure is schematically shown in Fig. 2(a) and consists of two 0.8-μm-thick InGaAsP passive core layers (with a bandgap cutoff wavelength of λ_g = 1.13 μm and a refractive index of 3.297), separated by a 0.8-μm-thick InP intermediate layer. If active functionalities are desired for the microring resonator, the upper core can be replaced by a structure whose equivalent refractive index maintains the phase matching condition with the passive underlying bus core. This requirement is met, for example, by a multi-quantum well active waveguide consisting of six 80-Å-thick 1% compressively strained InGaAsP (λ_g = 1.55 μm) quantum wells separated by 190-Å-thick InGaAsP (λ_g = 1.13 μm) barriers and sandwiched between two 190-nm-thick InGaAsP (λ_g = 1.13 μm) separate confinement heterostructure (SCH) layers (see Fig. 2(b)). In order to achieve a high confinement regime, both the bus and ring waveguides are deeply etched 0.6 μm beyond their core layers.

#230578 - $15.00 USD Received 17 Dec 2014; revised 4 Feb 2015; accepted 5 Feb 2015; published 20 Feb 2015

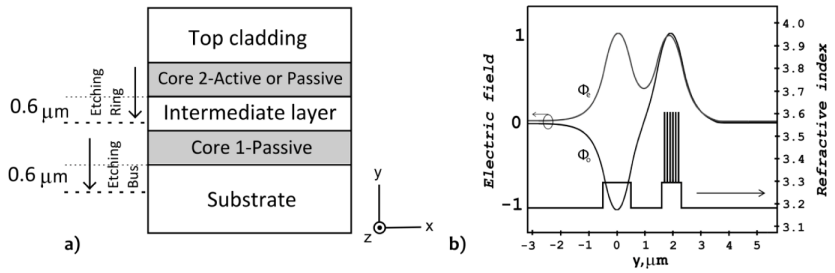

Fig. 2. (a) Layer structure of the vertically phase matched cores. (b) Refractive index and normalized mode profiles of the even Φe and odd Φo supermodes of the structure.

3.2 Disk bus waveguide

The passive standard ridge waveguide defined over the substrate (Fig. 1, section A) which distributes the light among other elements on the photonic circuit acts as the bus waveguide when approaching the microring resonator. This bus waveguide is then gently bent and laterally tapered in such a way that it becomes a disk bus waveguide, its fundamental mode being laterally confined by the outer sidewall and the bending effect itself (see Fig. 2, section B). Note that in the transition between the straight bus waveguide and the final disk bus waveguide there are some additional losses due to straight-to-bend and bend-to-bend connections. In Fig. 1, an S-bend waveguide is used to make the transitions between the straight waveguide and the tapered section that finally excites the whispering gallery mode. Related works [12] suggest that 0.3 dB would be a safe value for the loss in the S-bend and the taper. The shape and width of the whispering gallery mode in the bus disk greatly depends on the bend radius R_{bus}, which has to be large enough to wrap the upper microring and small enough to reach maximum mode-shape matching in the coupling region. A radius range from 100 to 400 µm provides a mode $1/e^2$ width range from 2 to 4 µm, respectively, for TE polarization (see Fig. 3). Due to the high index contrast of the structure, quadratic shaped lateral tapers as short as 30 µm provide mode transformation losses of under 0.1 dB.

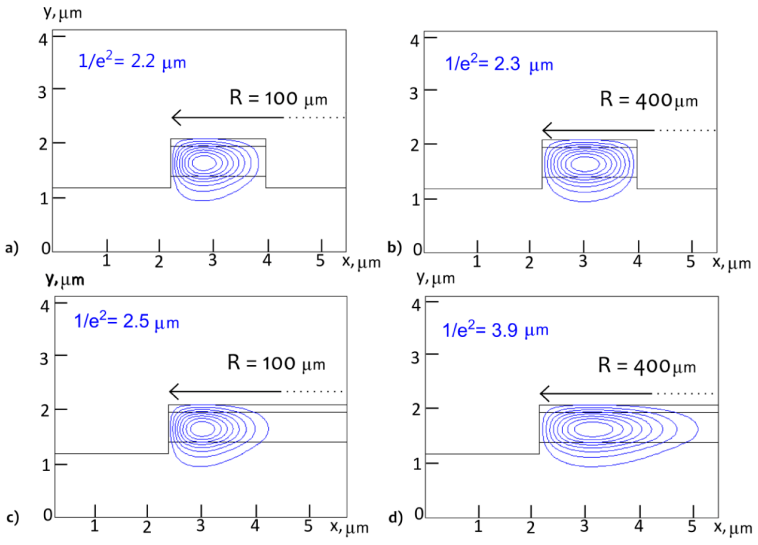

(1)

Fig. 3. Mode field distributions for TE polarization in a 2.5 um-wide passive ridge bus waveguide with (a) 100 µm and (b) 400 µm bend radius; (c) disk bus waveguide with 100 µm and (d) 400 µm bend radius.

#230578 - $15.00 USD Received 17 Dec 2014; revised 4 Feb 2015; accepted 5 Feb 2015; published 20 Feb 2015

3.3 The coupler

As soon as the disk bus mode reaches the coupling section, a fraction of the optical power is transferred to the ring waveguide by evanescent coupling (see Fig. 1, section C inset). Since the vertical position of the core layers is established by epitaxial growth, the overlap between the two modes and, therefore, the coupling factor k depends mainly on the vertical misalignment g and the mismatch in the size of the two optical modes. The width of the upper ring waveguide w is constrained by the single-mode propagation regime in the resonator, whereas the width of the mode in the disk bus waveguide is determined by its radius R (see Fig. 3).

The calculation of coupling factor k between the two waveguides calls for analysis of a three-dimensional structure of two vertically stacked waveguides, each with a different bending radius, which is a complicated task. The Finite Difference Time Domain (FDTD) method turned out to be very time-consuming for radii of more than 30 μm, proving impractical for our purposes. In view of weak coupling conditions, the simulation method used in this work is based on the discretization of the coupling region into differential steps, each one of them becoming a section of the structure (see Fig. 4(a)). The amount of optical power transferred between the bus and ring waveguides was then calculated in each differential section invoking coupled mode theory [13], followed by integration of all the calculated values along the structure. This method makes use of the unperturbed modes of the bus and ring waveguides which are obtained by matching the refractive index of the other core layer to that of the cladding. A commercial three-dimensional complex mode solver [14] was used to calculate the normal modes of both unperturbed waveguides, each of them calculated with its specific curvature radius (see Fig. 4(b)).

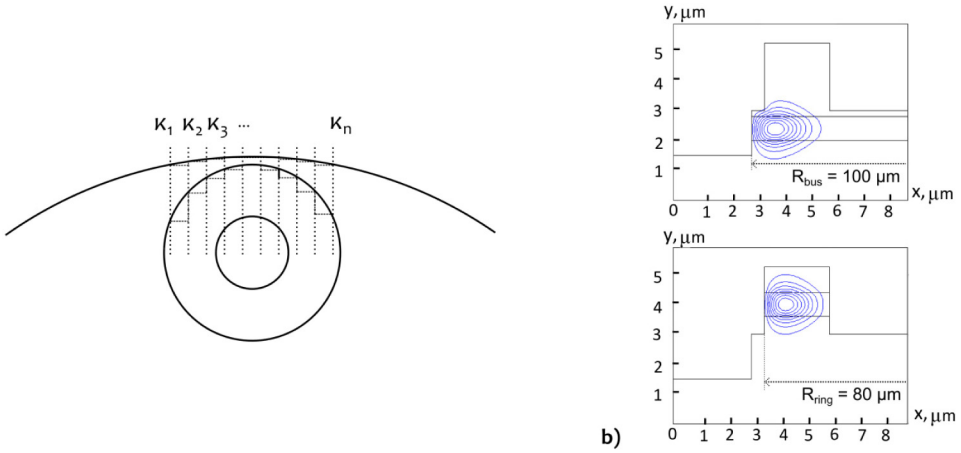

Fig. 4. (a) Step-like approximation of the circular profiles in the coupling region for coupled mode calculations. (b) Unperturbed mode distributions of the bus and ring waveguides with 100 and 80 μm curvature radii.

The geometrical analysis of Fig. 5 allows the estimation of the propagation angle for each mode, as well as an estimation of the exact transverse displacement determined by both, the radius difference of the waveguides and vertical misalignment g. Therefore, the local coupling value for the current section can be calculated by joining the unperturbed waveguide modes with these two geometrical parameters in a full vectorial film mode matching calculation [14]. Finally, the data set obtained is numerically integrated to obtain a good approximation of the total optical power transference between the two waveguides along the structure.

#230578 - $15.00 USD Received 17 Dec 2014; revised 4 Feb 2015; accepted 5 Feb 2015; published 20 Feb 2015

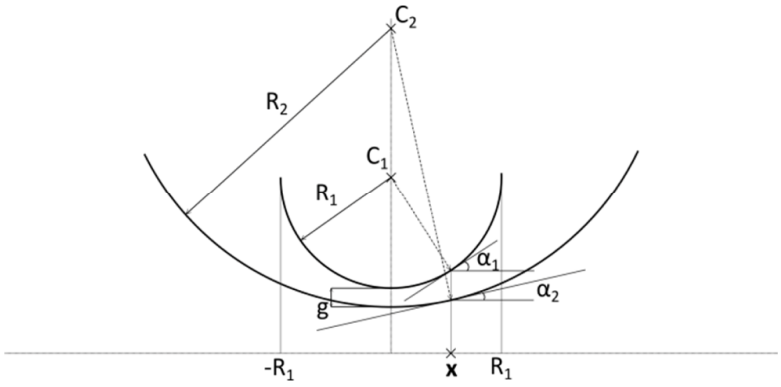

Fig. 5. Calculation of the propagation angles for the bus and ring modes.

Figure 6 shows the calculation results of k as a function of vertical misalignment g and ring radius R_{ring} for a ring waveguide width wring of 2.5 μm and a bus waveguide radius R_{bus} of 100 μm. As expected, larger radii provide higher power transfer, reaching values as high as 23% for a ring radius of 80 μm and a lateral gap of 0 μm. Typical values for the coupling efficiency in previous works range between 4 and 10% [9,15,16], therefore the proposed concept provides a safe range of values for this parameter. Note that submicron changes of the lateral gap result in rather large coupling variations. Note also that a lateral misalignment of 0.5 μm (typical for the current state-of-the-art mask alignment process) results in a 50% reduction in the coupling efficiency with respect to its maximum.

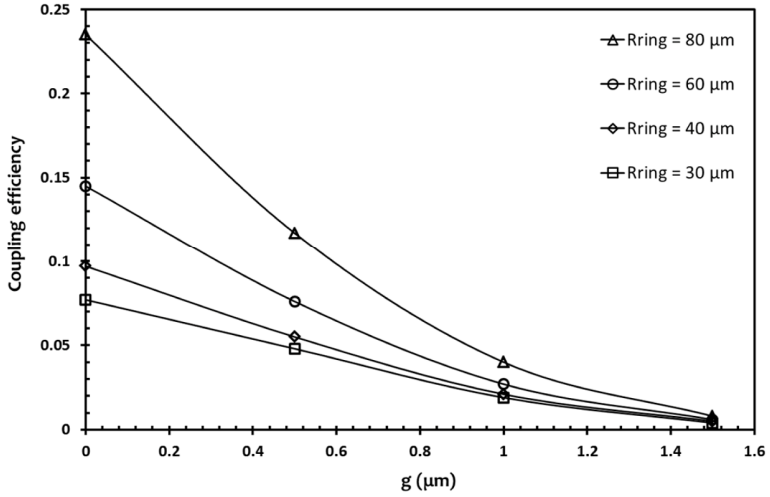

Fig. 6. Coupling coefficient k as a function of misalignment g and ring radius R_{ring}. A ring waveguide width wring of 2.5 μm and a bus waveguide radius R_{bus} of 100 μm are kept constant.

As shown in Fig. 3, larger bus waveguide radii provide wider passive modes, relaxing the submicron influence of the gap g. Figure 7 shows calculated coupling coefficient values for different bus waveguide radii ranging from 100 to 400 μm, as a function of misalignment g. The ring waveguide width w_{ring} and ring radius R_{ring} are kept constant through the calculations, with respective values of 2.5 μm and 60 μm. As the bus radius increases, so does the mismatch between the disk whispering gallery mode and the ring mode, thus lowering the coupling coefficients from around 14% to 8% for zero gap g. The advantage of larger radii lies in a smoother response of k to variations in g, which increase the design tolerance.

#230578 - $15.00 USD Received 17 Dec 2014; revised 4 Feb 2015; accepted 5 Feb 2015; published 20 Feb 2015

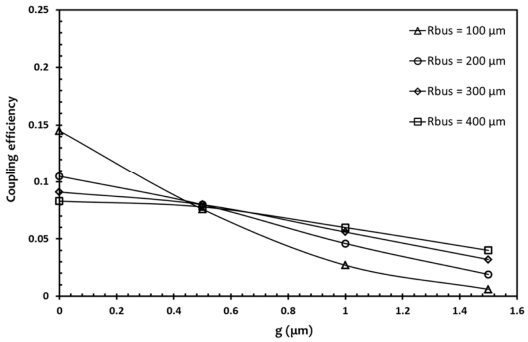

Fig. 7. Coupling coefficient k as a function of misalignment g and bus radius R_{bus}. Ring waveguide width w_{ring} (2.5 µm) and bus waveguide radius R_{bus} (60 µm) are kept constant.

The dependence of the coupling factor on the ring waveguide width w_{ring} was also analyzed. Calculations show little influence in the power transferred between the waveguides for ring widths between 2 and 4 µm. This is because the shape of the mode in the ring is determined by the bend radius rather than the width of the waveguide.

Both the high index contrast due to the deep etch and the lateral confinement provided by the smooth bend in the disk waveguide imply the low-loss propagation of higher order quasi-guided modes. Figure 8(a) shows the field distribution of the first order whispering gallery mode in the bus waveguide for a radius R_{bus} of 100 µm. Since the lateral taper in section B acts as a modal filter, it inhibits the propagation of high order modes in the device. However, the coupling efficiency of the system is reduced. Figure 8(b) shows the coupling factor between the fundamental ring mode and the bus first order mode; the coupling between the fundamental modes of the ring and bus waveguides is shown in gray for comparison. A gap of 0.5 µm and respective ring and bus radii of 80 and 100 µm, result in the first order mode in the disk receiving 37% of the power transferred to the bus waveguide. A straightforward technological approach to avoid this undesired behavior would be the etching of an inner sidewall for the bus waveguide inside the ring waveguide in order to reach single-mode propagation in the bus.

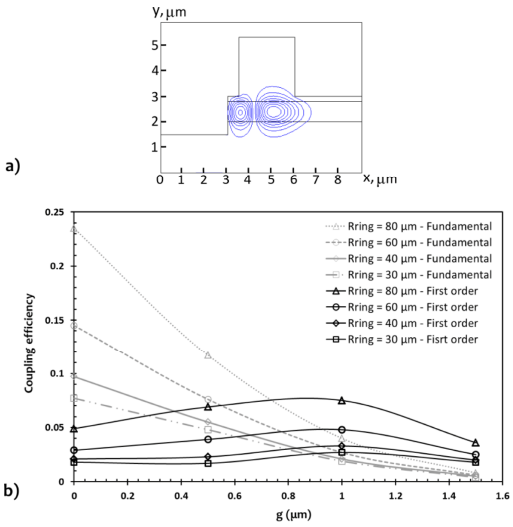

Fig. 8. (a) Field distribution of the first order mode in the disk bus waveguide section for R_{bus} = 100 µm, and (b) coupling coefficient k between the fundamental ring mode and the bus first order mode as a function of misalignment g and ring radius R_{ring}. Ring waveguide width w_{ring} (2.5 µm) and bus waveguide radius R_{bus} (100 µm) are kept constant

#230578 - $15.00 USD Received 17 Dec 2014; revised 4 Feb 2015; accepted 5 Feb 2015; published 20 Feb 2015

3.4 Ring waveguide optimization

Figure 9(a) shows the transverse structure of the ring waveguide in section D. The finite width of the ring waveguide compared to the infinite slab underlying bus core breaks the phase matching condition of the vertical layers. As a consequence, the even supermode of the structure is a weakly guided broad mode suffering large loss even for very small curvatures, while the odd supermode is a quasi-guided mode strongly confined in the ring waveguide. The field distribution of the two modes can be seen in Fig. 9(b) and (c).

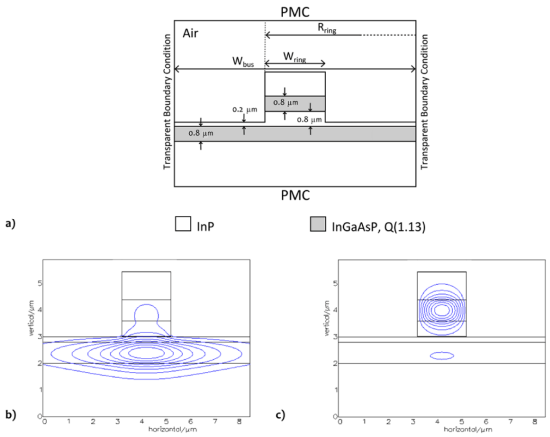

Fig. 9. (a) Cross-section of the simulated structure and detail of the boundaries used in the simulation: PMC stands for perfect magnetic conductor. (b) Modal field distribution of the fundamental eigenmode of the structure. (c) Modal field distribution of the first order eigenmode of the structure.

Again, a commercial three-dimensional complex mode solver [14] was used to simulate the proposed structure for different ring curvature radii. Transparent boundary condition [17] was used on both sides of the simulation window to absorb the power leaking from the bend and through the underlying slab waveguide, avoiding parasitic reflection. Since no light is radiated in the vertical direction, a perfect magnetic conductor was used as boundary condition for the top and bottom edges of the simulation window (see Fig. 9(a)).

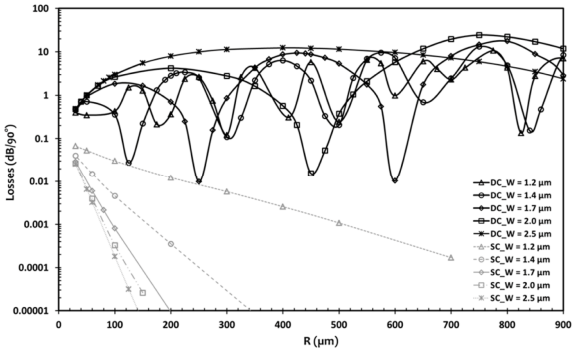

Fig. 10. (a) Simulated loss for the first order supermode of the structure as a function of bend radius for different rib widths and TE polarization. Bending loss for the structure resulting from the removal of the bus core is shown for comparison.

Figure 10 shows the total radiation loss (bending and leaky) for five different ring rib widths and for bend radii ranging from 30 µm to 1000 µm for TE polarization. Results for a standard ridge waveguide, fabricated on the same structure by removing the bus core layer, are also shown for comparison. In order to confirm these results, all the simulations were also

#230578 - $15.00 USD Received 17 Dec 2014; revised 4 Feb 2015; accepted 5 Feb 2015; published 20 Feb 2015

performed using FDTD, the results of which perfectly match those shown in Fig. 10. The behavior observed was totally different in the two situations. Bend losses in standard ridge waveguides are much lower and increase exponentially when the bending radius decreases, whereas in the double core structure, losses follow a remarkable oscillatory pattern, converging towards 0.1 dB/90° for radii below 100 μm. These loss levels in the microbend region are valid for the development of active microring devices in which round trip loss is compensated by the material optical gain, but are not low enough for passive filtering.

Most bending and leaky loss in the ring is produced by optical power radiation through the underlying slab bus core. By defining a broad rib waveguide for the bus core instead of leaving it as an infinite slab structure (see Fig. 11(a)), we avoid most of the radiation in the passive core plane while preserving the asymmetry between the waveguides. Calculated losses show values of under 0.2 dB/90° even for a radius of 30 μm (see Fig. 11(b)).

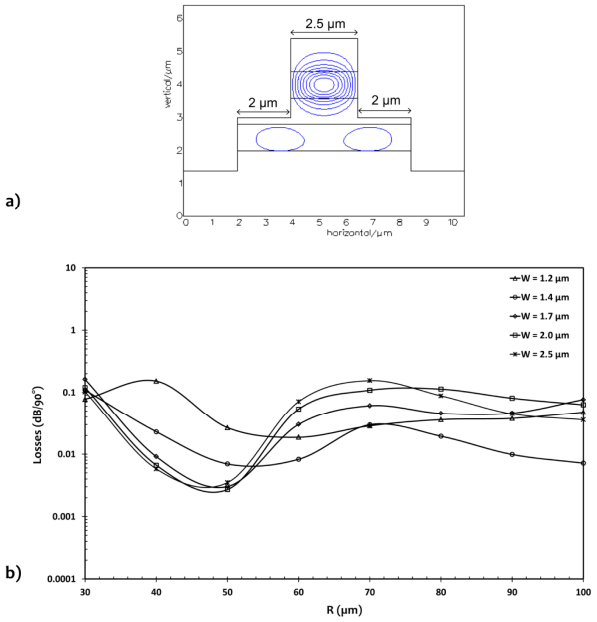

Fig. 11. (a) First order fully guided mode of the structure obtained by etching the bus core into a broad rib waveguide. (b) Calculations show bend losses lower than 0.2 dB/90° for this mode.

3.5 Microring design

Table 1 shows the free spectral range (FSR), full width at half maximum (FWHM) and quality factor Q of four different microring resonators designed with the theoretical parameters obtained previously. A double-rib structure was considered for the ring waveguide and a safe maximum loss of 0.1 dB/90° was used in calculations. These results are similar to the ones provided by other structures proposed so far [9,15,16]. We expect that this design may be used to fabricate high performance devices.

Table 1. Theoretical FSR, FWHM and Q provided by different design parameters for the proposed microring approach. Results are shown for the double etch structure, hence a safe maximum bend loss of 0.1 dB/90° has been considered.

w_{ring} (μm)	R_{ring} (μm)	R_{bus} (μm)	g (μm)	k	ring loss (dB/90°)	FSR (nm)	FWHM *(nm)*	Q
2.5	29	100	0.5	0.05	0.1	4	0.12	12325
2.5	39	100	0	0.1	0.1	3	0.15	10650
2.5	59	200	0.1	0.1	0.1	2	0.1	16112
2.5	80	100	0.5	0.12	0.1	1.5	0.08	19017

#230578 - $15.00 USD Received 17 Dec 2014; revised 4 Feb 2015; accepted 5 Feb 2015; published 20 Feb 2015

4. Conclusion

A new concept for the fabrication of integrated microring resonators is proposed. The approach is based on two vertically stacked phase matched core layers and avoids the need for complex fabrication processes such as electron beam lithography, wafer bonding or regrowth. Only one epitaxial growth and two single-side lithographic steps are needed to produce high performance microring resonators. The disk bus waveguide configuration used in the coupling region makes design of the upper ring waveguide extremely flexible. Its position and even its shape, defined in the second lithographic step, allow for a large coupling factor tuning range. The underlying high index core of the bus waveguide lends great asymmetry to the structure of the ring, resulting in an oscillatory behavior of the bending losses as a function of radius and ring waveguide width, providing convenient low loss minima. Furthermore, the definition of a broad rib waveguide in the bus core layer under the ring drastically reduces bending losses. Quality factors higher than 10000 are predicted by theoretical calculations. The structure is compatible with the integration of active-passive functionalities, allowing for the fabrication of microring lasers.

Acknowledgments

This research was supported by the Spanish Government project TEC2013-47264-C2-2-R and FEDER funds.

#230578 - $15.00 USD Received 17 Dec 2014; revised 4 Feb 2015; accepted 5 Feb 2015; published 20 Feb 2015